Chapter 6

Evaluating the Charge Transport Pathway Between DNA and the [4Fe4S] Cluster of Yeast DNA Polymerase δ

This work was done as part of a collaboration with Joseph Stodola, Carrie Stith, and Prof. Peter Burgers at the Washington University School of Medicine in St. Louis, Missouri.

P. Bartels identified possible mutant residues and performed all electrochemistry-based experiments. J. Stodola and C. Stith working with P. Burgers prepared all proteins, carried out basic characterization, and performed all *in vivo* experiments.

Introduction

A [4Fe4S] cluster in the C-terminal domain of yeast DNA polymerase δ is essential for the formation of an active multi-subunit complex and has recently been shown to be redox active in the presence of DNA (*1, 2*). Notably, electron transfer in Pol δ is thought to be primarily DNA-mediated, with electrons moving toward or away from the cluster through the π-stacked bases of the DNA in a process known as DNA-mediated charge transport (DNA CT) (*2, 3*). However, studies performed on a wide variety of other DNA-binding [4Fe4S] proteins that participate in DNA CT suggest that it is unlikely that electron transfer takes place directly between the cluster and the DNA (*4 -10*). Unfortunately, no structural data is available for this region in Pol δ, but these other cases may provide some useful general insights. Among these proteins, complete or partial structures are known for bacterial endonuclease III (EndoIII), MutY, archaeal XPD, and human DNA primase, and DNA-bound structures are also available for EndoIII, MutY, and mouse Dna2 (*4-10*). In all cases, the [4Fe4S] cluster is buried and thus shielded from solvent, and, for those with DNA-bound structures, the cluster is typically positioned at a distance of 15 Å or more from the DNA duplex (*8-10*). Aromatic residues have been shown to be critical for CT in EndoIII, and detailed mutagenesis studies in DNA primase reveal a string of tyrosine residue bridging the cluster and DNA (*11, 12*). Aromatic residues, specifically tryptophan and tyrosine, are well-known to act as bridges for electron hopping within proteins, and their use for this purpose in DNA-binding [4Fe4S] proteins is thus unsurprising (*13*).

In redox-active DNA-binding proteins, indirect electron transfer mediated by aromatic amino acid residues serves two main purposes. First, keeping the cluster away from the DNA may minimize the risk of DNA damaging Fenton chemistry if the cluster is degraded to release

free iron (*3*). Second, in order to communicate with one another in reversible long-range CT, all of these proteins must have similar potentials (*3*). Solvent exposure and proximity to the polyanionic DNA backbone are thought to be the primary factors in tuning redox potential, and thus these factors must be roughly equivalent between these proteins (*14, 15*). Pol δ has a measured redox potential that is indistinguishable from the well-characterized EndoIII in the same buffer conditions and is similarly unresponsive to in-solution oxidants and reductants, making it likely that the cluster environment is like that of other [4Fe4S] proteins that bind DNA (*1, 2*).

Previous work has shown that the oxidation state of the Pol δ [4Fe4S] cluster is important in regulating activity, with oxidation to the 3+ state markedly slowing DNA synthesis in a reversible manner (*2*). Such a redox switch would be very useful in responding to replication stress *in vivo,* especially in cases of oxidative stress. While *in vitro* work has been very useful in analyzing the redox capabilities of the cluster and its effect on enzymatic activity, addressing the actual function requires CT-deficient mutants that can be used in *in vivo* experiments. In these studies, we aimed to identify, prepare, and characterize several such mutants in Pol δ using *in vitro* techniques before proceeding to assess the sensitivity of yeast cells harboring these mutations to various stressors.

Materials and Methods

Protein Expression and Purification

Pol δ DV (D520V) and the mutants W1053A and Y1078A were prepared using a previously published yeast overexpression system (*16*). PCNA was prepared by overexpression in yeast, while RFC and RPA were overexpressed in *E. coli* following previous protocols (*17-19*).

DNA Preparation

Thiol-modified DNA was prepared on an Applied Biosystems automated DNA synthesizer using a 3′ thiol modifier phosphoramidite and standard reagents from Glen Research. Unmodified DNA was purchased from IDT. All DNA sequences were purified by HPLC as described previously (*2*), and annealed in 1:1 molar ratios for electrochemistry. The sequences used were as follows:

20-mer 3′ thiol: 5′ - GCT GTC GTA CAG CTC AAT GC - 3′ - $(CH_2)_2O(CH_2)_3SH$

38-mer: 5′ - TAA CAG GTT GAT GCA TCG CGC TTC GGT GCT GCG TGT CT - 3′

49-mer: 5′ - GCA TT**G** AGC TGT ACG ACA GCA GAC ACG CAG CAC CGA AGC GCG ATG CAT C - 3′

DNA replication assays utilized the single-stranded plasmid M13mp18 DNA annealed to a 31-mer primer in a 1:1 ratio (5′ at 90 °C followed by slow cooling to RT). The primer was complementary to positions M13mp18 positions 6265-6234, and had the following sequence:

5′ - GAC TCT AGA GGA TCC CCG GGT ACC GAG CTC G - 3′ (1)

For activity assays, a 5′ ^{32}P label was appended to the primer before annealing using T4 polynucleotide kinase (PNK) in PNK buffer with [γ-^{32}P] ATP. Product sizes were determined using HincII-digested M13mp18 RFII DNA and 2 log DNA ladder, radiolabeled with T4 PNK following dephosphorylation by calf intestinal alkaline phosphatase (CIAP; 60 minutes, 37 °C).

DNA and enzymes were purchased from New England Biolabs (NEB), and radiolabeled ATP was from Perkin Elmer.

Electrochemical Characterization on DNA-Modified Gold Electrodes

Electrochemical characterization was performed on multiplexed chips with 0.015 cm^2 electrode area (*20*). Loosely-packed DNA self-assembled monolayers (SAMs) were formed by incubating 25 μL of 25 μM duplexed DNA on the electrode overnight, after which electrodes were rinsed 3-5 times in phosphate buffer (5 mM sodium phosphate, pH 7.5, 50 mM NaCl) and backfilled for 45 minutes with 1 mM 6-mercapto-1-hexanol in the same buffer containing 5% (v/v) glycerol. After backfilling, electrodes were extensively rinsed in phosphate buffer followed by protein storage buffer (30 mM HEPES, pH 7.4, 350 mM NaAc, 1 mM DTT, 0.5 mM EDTA, 10% glycerol, and 0.01% decaethylene glycol monododecyl ether), and the absence of electroactive impurities was confirmed by cyclic voltammetry (CV).

Electrochemical experiments used a standard 3-electrode cell consisting of a Au working electrode with a Ag/AgCl reference electrode in 3 M NaCl (BASInc), and a 1 mm diameter Pt wire as the counter electrode (Lesker). Potentials were converted from Ag/AgCl to NHE by adding 212 mV to the potential measured by Ag/AgCl (*2*). Because the [4Fe4S] absorbance was too low to determine concentration, Pol δ mutant concentrations in electrochemical experiments are reported as total protein concentration determined by Bradford assay. For unmodified Pol δ DV, [4Fe-4S] cluster concentration was determined by UV-visible spectroscopy using an extinction coefficient of 13000 $M^{-1}cm^{-1}$ at 400 nM, and a cluster loading of ~85% was determined by dividing cluster concentration by total protein concentration as determine by Bradford assay. For comparison with mutants, similar loading levels were assumed and equivalent amounts of loaded protein were added to electrodes. BSA and reagents were included

in kits purchased from Thermo Scientific, and UV-vis spectra were taken on a Cary Varian instrument using 100 μL quartz cuvettes (STARNA Cells).

Electrochemistry was performed using 500 nM Pol δ DV (unmodified or mutant) in combination with 5.0 μM PCNA, 80 μM dATP and 8 mM $MgAc_2$ in storage buffer (30 mM HEPES, pH 7.4, 350 mM NaAc, 1 mM DTT, 0.1 mM EDTA, 10% glycerol v/v, and 0.01% w/v decaethylene glycol monododecyl ether). Surfaces were scanned by CV (100 mV/s scan rate) and square wave voltammetry (SQWV; 15 Hz frequency and 25 mV amplitude) once per hour for several hours.

Activity Assays with Oxidized and Reduced Pol δ Mutants

Unless otherwise noted, bulk electrolysis was carried out in an anaerobic glove bag (95% N_2/5% H_2) using droplet electrochemistry (30-40 μL 190 nM sample diluted into degassed storage buffer) on Au rod electrodes of 0.0314 cm^2 electrode area (Pine Research Instrumentation). Oxidation was performed using a potential of 0.412 V vs NHE, while reduction was done at -0.188 V. Oxidation yields were estimated by taking the difference between the total charge obtained in the presence of Pol δ and that generated by electrolysis with buffer alone.

140 μL reaction mixes (0.1mg/mL BSA, 80 μM each dNTP, 500 μM ATP, 2.0 nM M13mp18 with a ^{32}P-labeled primer, 8.0 mM $MgAc_2$, 500 nM RPA, 5.0 nM RFC and 50 nM PCNA in 50 mM Tris-HCl with 50 mM NaCl, pH 7.8) were prepared inside the glove bag. All buffer components were purchased from Sigma-Aldrich.

PCNA was loaded onto primed ends by incubation with RFC (1′, 30 °C), and reactions were started by addition of Pol δ to 2 nM. Reactions were run at 30 °C, and 20 μL aliquots were removed at the specified time points and quenched with 10 μL stop mix (10 mM EDTA and 0.1% v/v SDS, final concentrations). Samples were counted on a liquid scintillation counter and

dried on a speed vacuum before being dissolved in alkaline gel buffer (500 mM NaOH, 10 mM EDTA) with 6x alkaline loading dye (300 mM NaOH, 6.0 mM EDTA, 18% Ficoll w/v, 0.25% xylene cyanol w/v, and 0.15% bromocresol green w/v) diluted to 1x in buffer. Equivalent amounts of radioactivity were loaded onto a 1% alkaline agarose gel and run at 30 V for 14-15 hours. Gels were neutralized in 7% TCA w/v in water (30 minutes, RT), dried, and imaged on a Typhoon phosphorimager. Gels were quantified using ImageQuant software (GE Healthcare). Because oxidation affected the mutants differently (described below), the total amount of DNA synthesis (identified as radioactivity above unextended primer) was compared.

***In Vivo* Assays**

Yeast strains containing either WT or mutant Pol δ were treated with exogenous agents to test the response to replication stress. Treatments included UV irradiation, camptothecin, and hydroxyurea, and treated cells were spot plated for an assessment of growth. To test sensitivity to oxidative stress, a mutant yeast strain defective in glutathione synthase (Δ*gsh*) was prepared, and cells were treated with either hydrogen peroxide (2 mM) or menadione (50 mM). Analysis was the same as for more generic treatments.

Results

Identification of Putative CT-Relevant Residues in Pol δ and Purification of Mutants

Sequence alignments of the catalytic subunits of Pol δ and Pol α (Pol3 and Pol1, respectively) were used as first step in identifying conserved aromatic residues that might be involved in the Pol δ CT pathway. Because no structure of Pol δ containing the C-terminal domain that harbors the cluster exists, we relied upon a structure of the Pol α CTD/B-subunit complex (PDB ID 3FLO) to estimate distances between the cluster and possible CT-relevant residues. To facilitate this analysis, we limited ourselves to residues conserved between both Pol δ and Pol α. It should be noted that Pol1 differs from Pol3 in the spacing of ligating cysteine residues, and the structure used contains zinc in place of a [4Fe4S] cluster (*21*), so some limitations to this strategy are present. If anything, these factors would lead to an overestimation of distances; nonetheless, given a lack of alternatives and the high degree of conservation in this region between the B-family polymerases, we considered the Pol1 structure sufficient for our purposes. Proceeding with this strategy, we identified two conserved aromatic residues within 15 Å of the Pol1 zinc (and thus likely closer in Pol3 with an intact [4Fe4S] cluster): W1053 and Y1078.

Notably, these residues are on opposite sides of the cluster, with W1053 facing the external environment and Y1078 more deeply buried (Figure 6.1). Thus, if these residues are involved in CT, they are likely to represent redundant pathways rather than a single, coherent path between DNA and the cluster; alternatively, one or both may be entirely uninvolved in CT. While the position of DNA relative to the cluster is unknown, the buried position of Y1078 makes this residue unlikely to be in direct contact with the DNA; however, it could still serve as the final residue in a string originating elsewhere. To maximize our chances of finding relevant

residues and to address this latter point, we also targeted Y1035, a residue in one of the alpha helices midway between the CysA zinc finger and the CysB [4Fe4S] cluster site (*1, 21*).

Once identified, constructs were designed with W or Y → A mutations in Pol δ DV, and all three mutants were overexpressed in yeast and purified according to standard protocols. Yields were lower than expected, although FPLC traces confirmed that intact 3-subunit complexes did form for both W1053A and Y1078A (Figure 6.2). Nonetheless, the proportion of degraded complexes was considerably higher than seen in unaltered Pol δ DV, and yields of intact complexes were too low to obtain useful quantities of Y1035A. The low yields and tendency of these mutants to degrade even when purified under anaerobic conditions suggested that the alanine substitution was likely perturbing structural integrity to some extent, although complexes could clearly still form. Supporting the fully intact nature of these collected fractions, the major peak also included absorbance at 410 nm, characteristic of [4Fe4S] clusters (Figure 6.2). Since we were still able to obtain intact complexes for W1053A and Y1078A at ~500 nM, we decided to proceed to assess their effects on activity and electrochemical properties in addition to their effect on cell viability under different stress conditions.

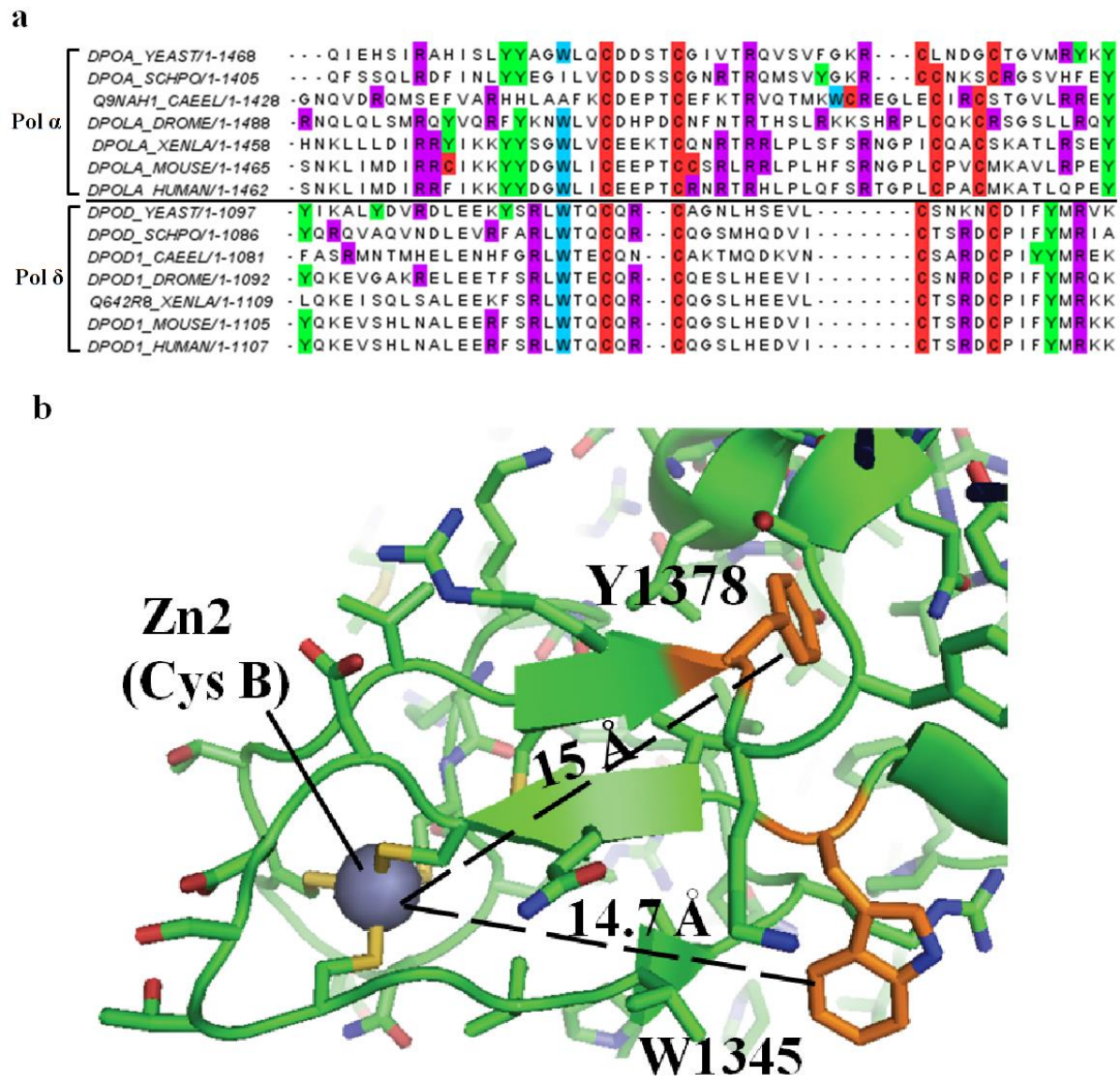

Figure 6.1 Identification of possible CT-relevant residues in Pol δ using sequence alignments and a Pol α C-terminal domain X-ray crystal structure (*21*). (a) Sequence alignments of Pol α and Pol δ from a variety of organisms. Cluster-ligating cysteines are highlighted in red, tyrosine in green, tryptophan in blue, and arginine in violet. Arginine is included to illustrate the proximity of a disease-relevant mutation in human Pol δ (ref. *27*). (b) Yeast Pol α C-terminal domain structure (PDB ID 3FLO) highlighting Y1378 and W1345, which correspond to Y1078 and W1053 in yeast Pol δ. Notably, both residues are within electron tunneling distance (~15 Å) from a zinc that occupies the CysB site in this structure, and these distances would be even shorter if the native [4Fe4S] cluster were present.

Characterization of Pol δ Mutants

Yeast strains containing Pol δ W1053A or Y1078A exhibited unperturbed growth, indicating that these mutants were able to form complexes effectively enough to support normal DNA replication. To see if replication stress inducers had a differential effect on these strains, cells were subjected to UV, camptothecin, and hydroxyurea treatment and spot plated (Figure 6.3; only hydroxyurea treatment is shown). Among these treatments, the Y1078A strain showed slight sensitivity to 75 mM hydroxyurea, although neither mutant was sensitive to lower concentrations or to any other stressor applied.

In an effort to accurately determine cluster loading levels, both mutants were concentrated to the extent possible (500 nM) for UV-visible spectroscopy (Figure 6.4). A clear absorption peak at 280 nm attributable to aromatic and thiolated amino acid residues was present, and the absence of elevated absorption at 800 nm indicated that aggregrates were not forming. At these concentrations, the low extinction coefficient of the cluster (13000 $M^{-1}cm^{-1}$ at 400 nm) makes the presence of a peak difficult to discern. To work around this problem, absorbance at 280 nm was normalized to 1 using an unmodified Pol δ DV spectrum; BSA, which should have no absorbance in the 400 nm region, was included as a control. When this analysis was carried out, both mutants show absorption elevated beyond BSA that is generally shaped like the peak in unmodified Pol δ DV, supporting similar cluster loading. However, with absolute absorbance so low, these results are not definitive. Although not quantitative, the best evidence for comparable cluster loading in the mutants remains the FPLC evidence for the formation of 3-subunit complexes with 410 nm absorption.

In vitro, both Pol δ DV mutants remained active in standard DNA replication assays on primed ssM13mp18 plasmid DNA (Figure 6.5). They did, however, exhibit lower processivity

than unaltered Pol δ DV, although native activity could be restored by adding a 10-fold molar excess of PCNA (Figure 6.5). Pol δ typically requires only stoichiometric amounts of PCNA to completely extend a primed ssM13mp18 plasmid, and these results indicate that the interaction of these mutants with PCNA is disrupted to some extent. PCNA binding involves the CysA zinc finger at the other side of the C-terminal domain from the [4Fe4S] cluster (*1*), so these results suggest that this entire region of the protein has undergone some reorganization upon these mutations. That excess PCNA can compensate demonstrates that PCNA binding remains possible, and suggests that, although structurally perturbed, the mutants remain in intact 3-subunit complexes.

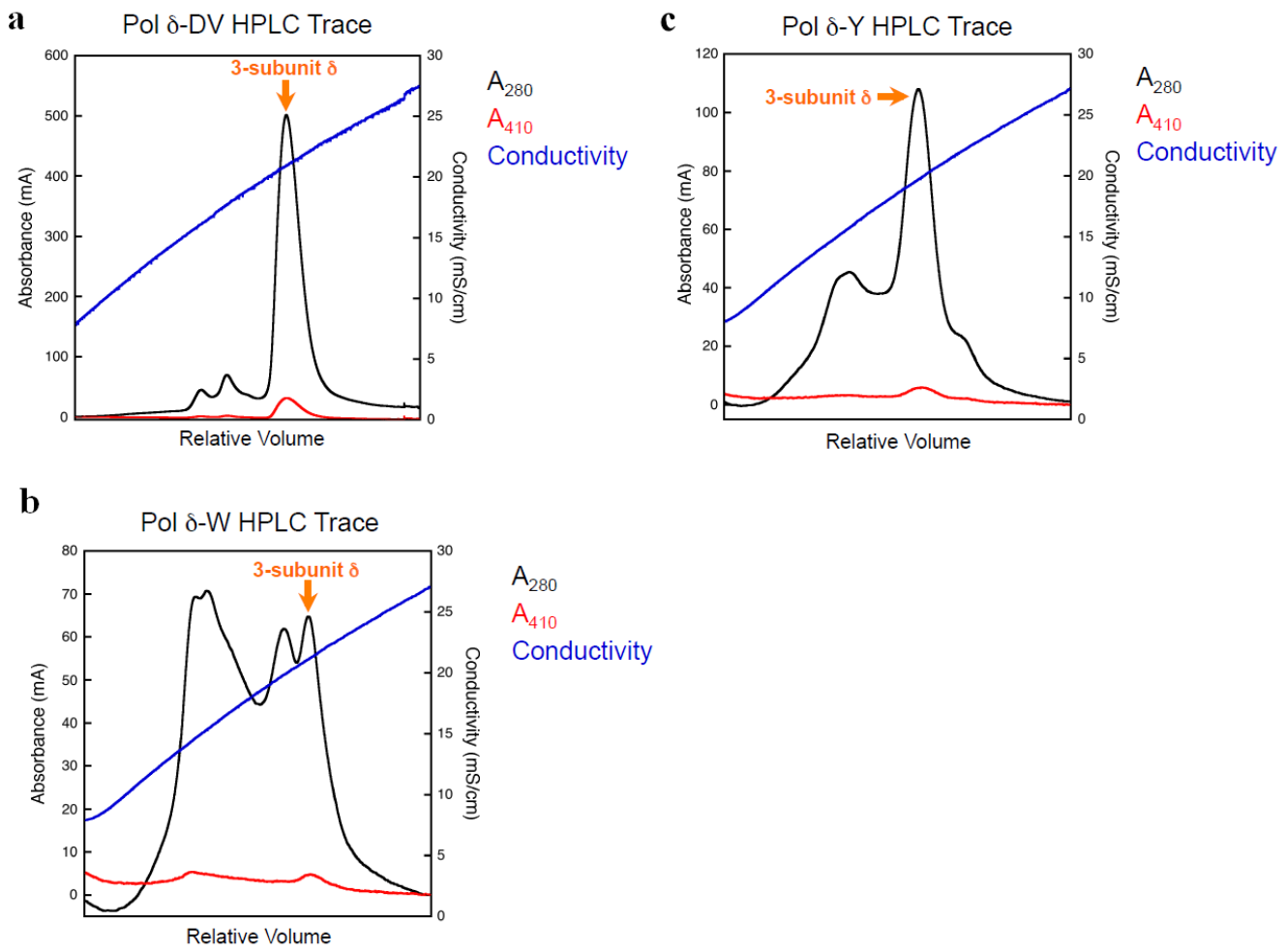

Figure 6.2 HPLC traces from Pol δ purification on a MonoS column in a 150 – 750 mM NaAc gradient. (**a**) Pol δ DV without any additional mutations elutes primarily as a three-subunit complex that contains substantial absorbance at 410 nm associated with the presence of a [4Fe4S] cluster. (**b**, **c**) Preps from Pol δ DV W1053A (**b**) and Y1078A (**c**), in contrast, are lower yielding (note the scale) and contain a much higher proportion of degraded complexes eluting at earlier time points, indicative of lower stability. Despite low stability, some absorbance at 410 nm remains visible, supporting the assumption that intact complexes bind a [4Fe4S] cluster.

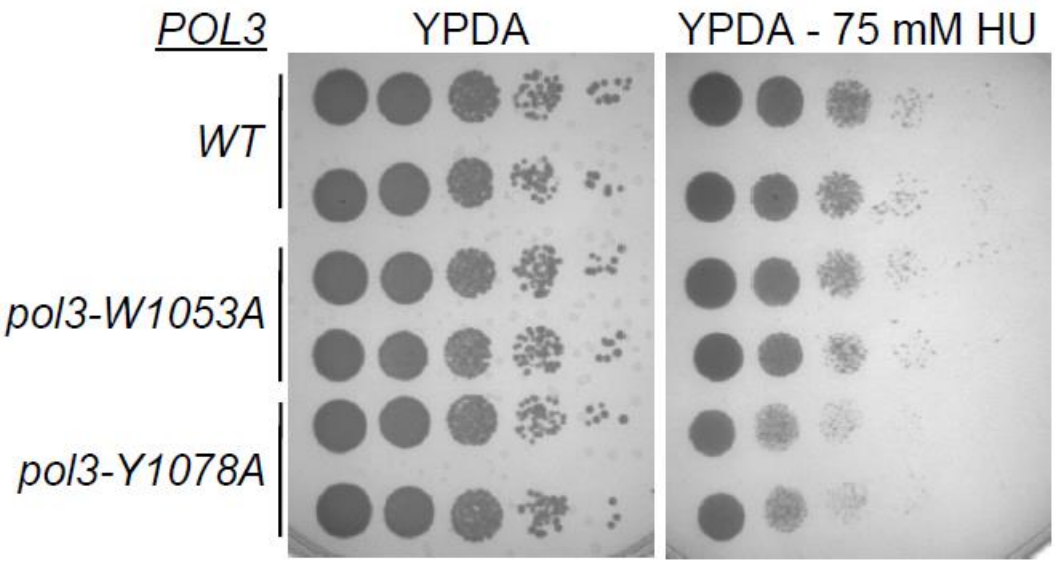

Figure 6.3 Growth of budding yeast containing WT, W1053A, or Y1078A Pol δ on YPDA medium with and without 75 mM hydroxyurea. Y1078A showed a slightly enhanced sensitivity to hydroxyurea, although neither mutant was sensitive to UV irradiation or camptothecin treatment (not shown).

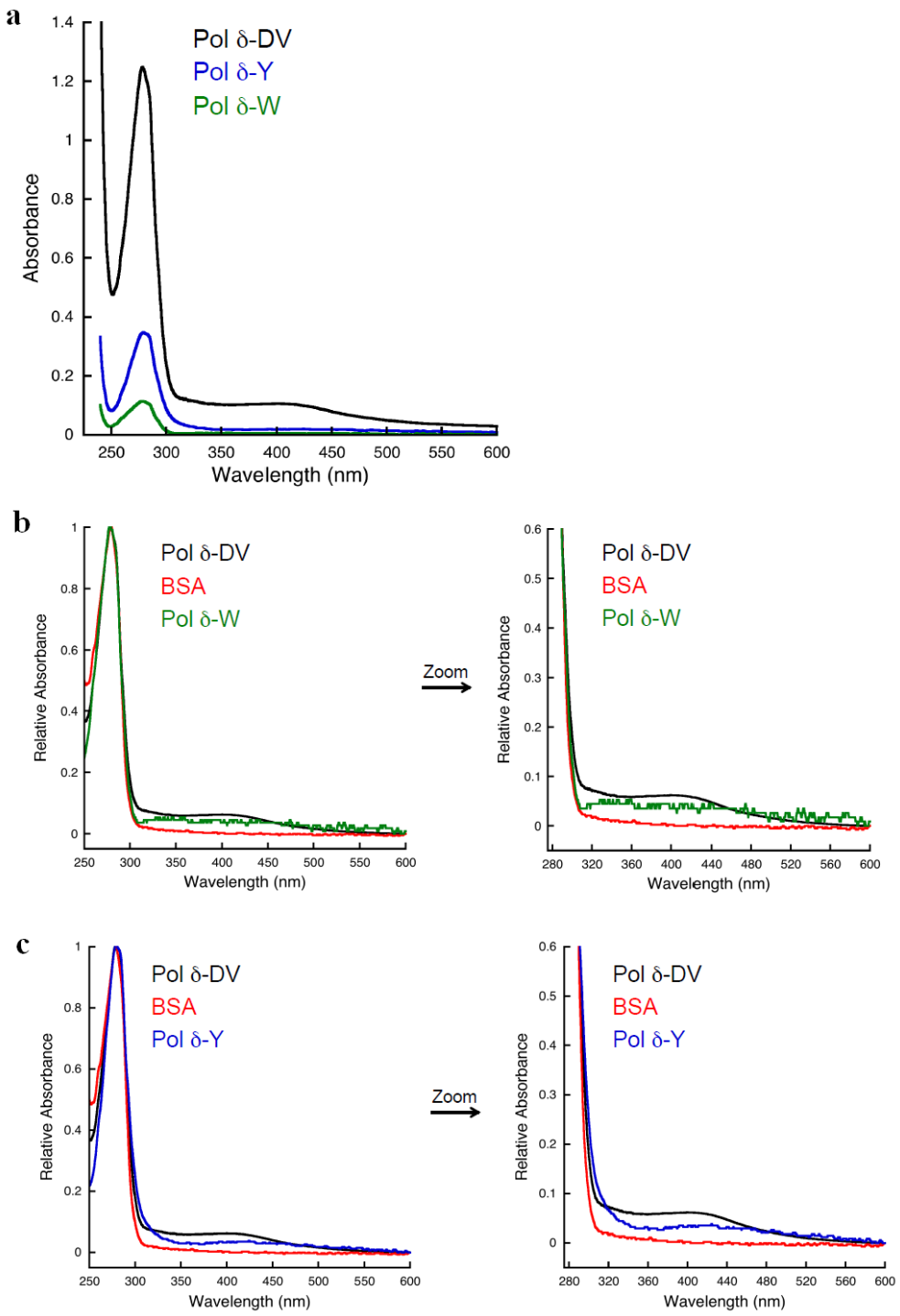

Figure 6.4 UV-visible spectra of Pol δ DV and the mutants W1053A and Y1078A. (**a**) Both mutants were much more dilute than Pol δ DV, making [4Fe4S] cluster concentration difficult to calculate. (**b**, **c**) To see if [4Fe4S] cluster absorbance at 410 nm was present, spectra were normalized to A280 and compared with BSA, which does not bind a cluster. Although not ideal, this analysis does suggest [4Fe4S] binding, in agreement with the fact that both form intact complexes and show 410 nm absorbance by HPLC during purification.

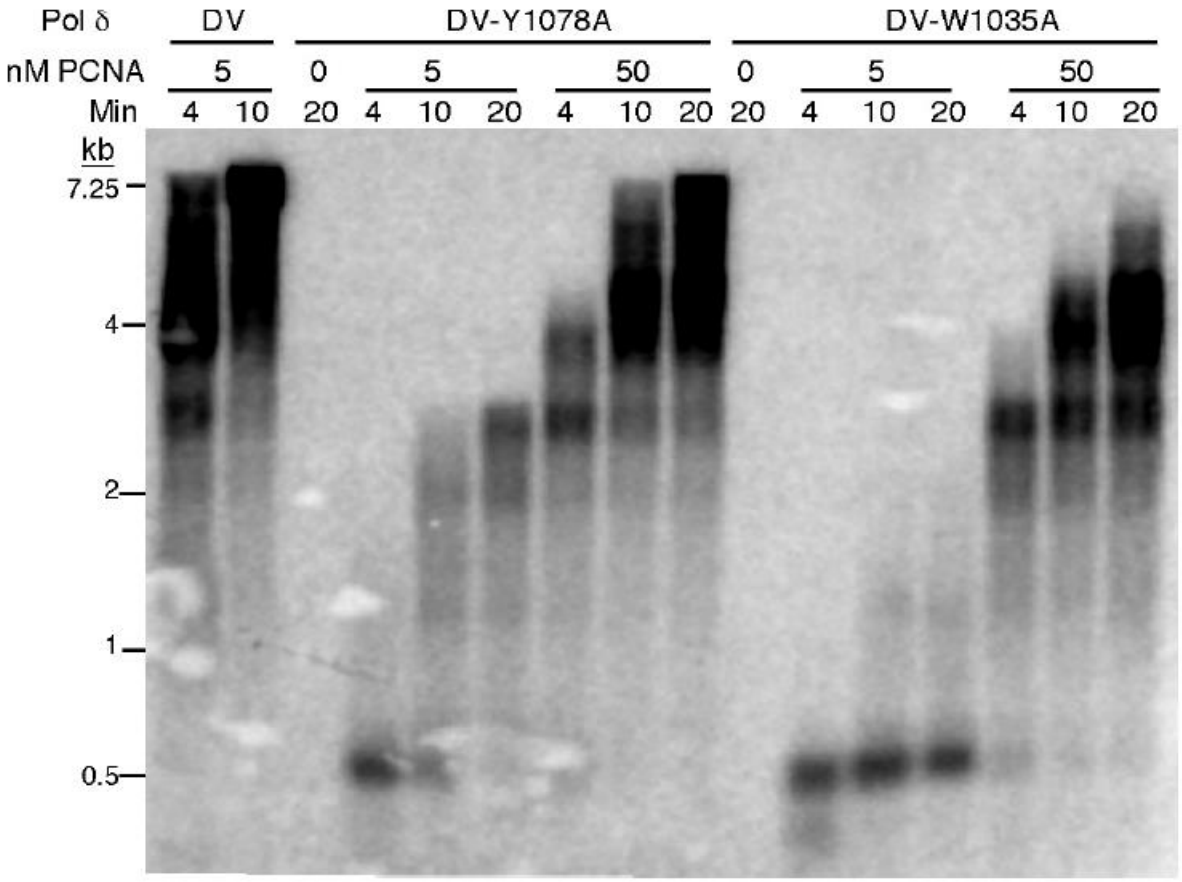

Figure 6.5 Primed ssM13mp18 plasmid DNA replication by Pol δ variants in a standard lagging strand replication assay. Pol δ DV (left) shows complete replication of the 7.3 kb substrate by 10 minutes with stoichiometric PCNA. Both Y1078A (center) and W1053A (right) are less processive, and require a 10-fold excess of PCNA for complete replication. Notably, the processivity defect is more pronounced in W1053A, which also appeared less stable during purification.

Electrochemical Characterization of Pol δ Mutants

With basic cell growth assays and biochemical characterization completed, we next proceeded to investigate the redox properties of these mutants using electrochemistry on DNA-modified gold electrodes. All electrochemical experiments were run on multiplexed chips in parallel with Pol δ DV (Figure 6.6). To maximize signal size at these low concentrations, we used 500 nM Pol δ pre-mixed with 5.0 μM PCNA, 80 μM dATP, and 8 mM $MgAc_2$. CT-proficient Pol δ DV gives substantial signals under these conditions (~5-10 nC maximum CV peak charge), and signals remain reliably detectable at least down to a tenth of this size (*2*). Thus, we reasoned that these conditions should be sufficient to observe the mutants even if they were nearly completely CT-deficient relative to WT. However, given that both mutants showed lower processivity in activity assays and were thus less likely to bind DNA as effectively as unmodified Pol δ DV, one half of each chip contained DNA with a 3′ ddC substrate trap; the remaining quadrants contained unmodified DNA.

Small but quantifiable electrochemical signals occur with both mutants; the midpoint potentials are 121 ± 4 mV and 120 ± 3 mV versus NHE for W1053A and Y1078A, respectively. As expected, the potentials are very similar to Pol δ DV (113 ± 5 mV). Because the relatively large CV capacitance can impede signal quantification and make comparison difficult for small signals, SQWV, which minimizes background current, was used for this purpose instead. By SQWV, the W1053A and Y1078A peak areas are 21 ± 7 % and 25 ± 4 % of unmodified Pol δ DV signals (Figure 6.6). Interestingly, no obvious differences occurred in the presence of the ddC substrate trap, although signal sizes were somewhat less variable on this DNA. This result can most likely be attributed to the saturation of available DNA with protein: loosely-packed monolayers contain 0.2 – 0.3 pmol DNA per electrode (*22*), while 10 pmol of Pol δ was present.

Like Pol δ DV, the Y1078A signal grows in over time, although it never reaches the same extent (Figure 6.7). In contrast, W1053A remains small and even decreases over time, possible indicative of sample degradation over extended time in aerobic conditions.

Interestingly, after overnight incubation, a secondary, irreversible reductive peak centered around -40 mV versus NHE develops in Y1078A; at the same time point, the W1053A signal is too small to see if the same additional peak develops. In unstable human MUTYH mutants, an irreversible peak at the same potential is attributable to oxidative degradation of the [4Fe4S] cluster to the $[3Fe4S]^{+}$ state (*23*). Such degradation in the less stable Pol δ mutants is a reasonable explanation for this peak, although the low concentrations of these mutants precluded UV-visible and EPR spectroscopic identification. In MUTYH mutants, cluster degradation is dependent on O_2, and the secondary peak can be significantly amplified by bulk electrolysis in an aerobic environment (*23*). Given the impossibility of spectroscopic analysis in the case of Pol δ DV Y1078A, we undertook aerobic bulk electrolysis as an alternative to see if the pattern matched that of MUTYH (Figure 6.8). As a control, we repeated this experiment with unmodified Pol δ DV (Figure 6.8). In these experiments, UV-visible spectra were taken before and after oxidation, and one half of the sample was left untreated and incubated on a multiplexed chip. CV and SQWV scans were taken of both samples on a multiplexed chip before and after electrolysis. After 1 hour, aerobic oxidation had reached its maximum extent, and the oxidized sample was transferred back to the multiplexed chip once a UV-visible spectrum had been taken. Immediately after electrolysis, the Y1078A signal was slightly smaller than the untreated control, although this may have been in part due to minor sample loss. Despite sample loss, the secondary peak was proportionally larger relative to the main peak at this point (Figure 6.8). All signals disappear entirely within 2 hours of incubation in the oxidized sample; signals in the untreated

sample gradually decrease, but not to the same extent (Figure 6.8). UV-visible spectra taken after electrolysis show an increase in absorbance at 800 nm, and the entire spectrum is U-shaped, consistent with aggregation (Figure 6.8). When repeated with unmodified Pol δ DV, the UV-visible spectrum post-electrolysis shows a general increase in cluster absorbance associated with oxidation with no evidence for aggregation (Figure 6.8). Furthermore, electrochemical signals remain indistinguishable from untreated sample even after extended incubation, and no peak indicative of $[3Fe4S]^{+}$ cluster is observed. Overall, these results can best be explained as a difference in stability between unmodified Pol δ DV and the Y1078A mutant. The cluster in unmodified Pol δ DV is stable in air even when oxidized to the $[4Fe4S]^{3+}$ state, likely as a result of tight binding with the B-subunit. In contrast, Y1078A, although capable of forming intact complexes, is structurally perturbed, making the cluster more susceptible to oxidative degradation in air. The loss of signal and evidence for aggregation suggest that the cluster in this mutant degrades upon oxidation, causing complexes to come apart and aggregate. Pol3 is known to be aggregation-prone in the absence of B-subunits, providing further support for our assessment of these results.

Notably, absent forced oxidation by bulk electrolysis, cluster degradation as observed by electrochemistry takes several hours to develop in the Pol δ mutants, with Y1078A appearing as the more stable of the two. This observation suggests that, while these mutants are less stable than WT Pol δ, at least Y1078A is stable on short time scales. Overall, CT deficiency is apparent in both mutants, although whether it is the result of involvement of the residue in the CT pathway or simply complex degradation is ambiguous. Since Y1078A appears somewhat more stable than W1053A, however, a case can be made that this residue is part of a CT pathway. Even with Y1078A, however, some signal loss due to complex degradation cannot be excluded.

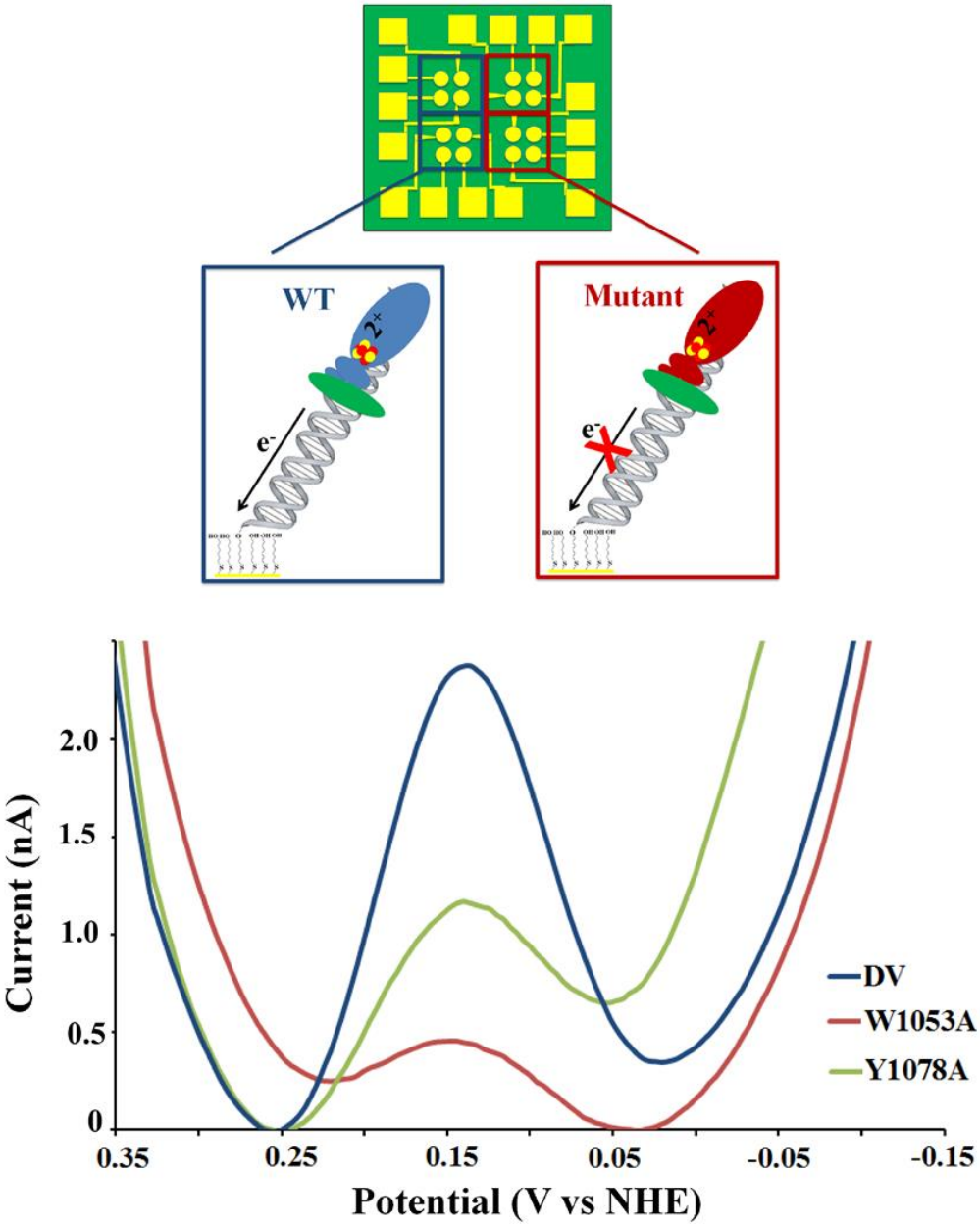

Figure 6.6 Square wave voltammetry (SQWV) of Pol δ DV and the W053A and Y1078A mutants. Polymerase variants were incubated in parallel on a multiplexed chip (**top**), and each quadrant contained 25 µL of 500 nM Pol δ DV, 5.0 µM PCNA, 80 µM dATP, and 8.0 mM $MgAc_2$ in storage buffer (20 mM HEPES, pH 7.4, 350 mM NaAc, 1 mM DTT, 0.5 mM EDTA, 10% glycerol v/v, 0.01% decaethylene glycol monododecyl ether v/v). Both mutants showed marked deficiency in redox activity relative to Pol δ DV, with signal area only 20-25% of the unmodified protein (**bottom**). SQWV scans run from left to right, and were taken at 15 Hz frequency and 25 mV amplitude.

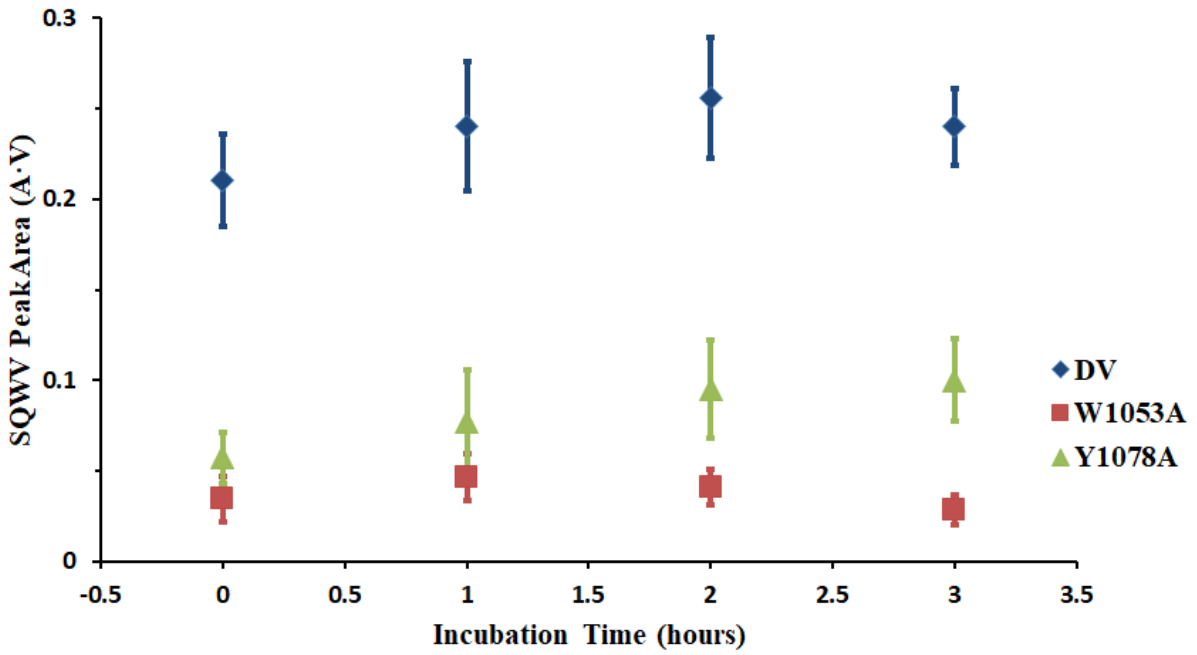

Figure 6.7 SQWV signal growth and stability over time for 500 nM Pol δ DV and the mutants W1053A and Y1078A. Pol δ DV equilibrates rapidly and the signal remains stable for several hours. Y1078A has a similar patter, although signals are much smaller and equilibration is more prolonged. W0153A plateaus early, after which the signal steadily decreases. The loss of signal in W1053A is most likely attributable to oxidative degradation in the aerobic environment. Experiments were performed in storage buffer (20 mM HEPES, pH 7.4, 350 mM NaAc, 1 mM DTT, 0.5 mM EDTA, 10% glycerol v/v, 0.01% decaethylene glycol monododecyl ether v/v) with 5.0 μM PCNA, 80 μM dATP, and 8.0 mM $MgAc_2$.

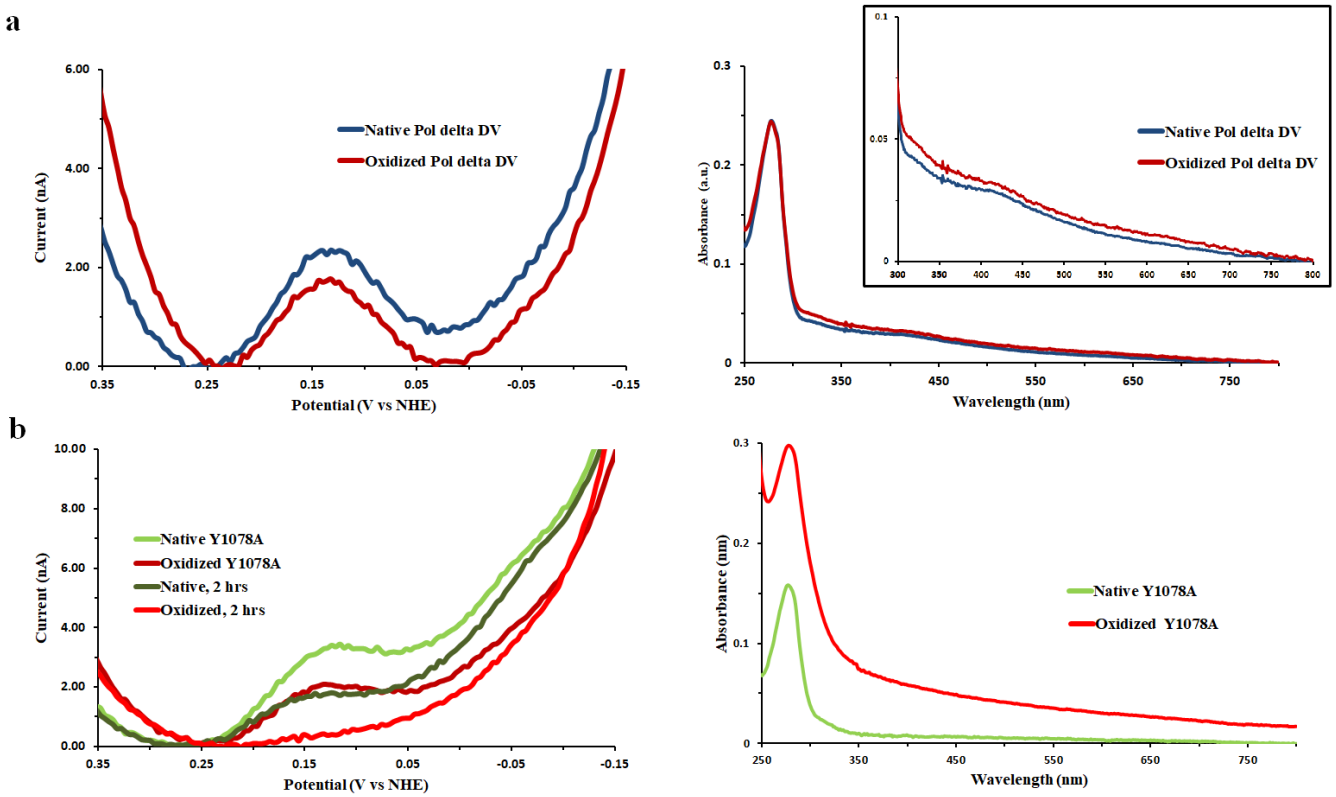

Figure 6.8 SQWV (left) and UV-visible spectroscopy (right) of untreated and aerobically oxidized Pol δ DV (**a**) and Y1078A (**b**). (**a**) Oxidation by bulk electrolysis (0.412 mV vs NHE) in air did not result in any appreciable changes in Pol δ DV electrochemistry (the smaller signal can be attributed to a minor loss of sample), and the UV-visible spectrum was unaltered except for a broad increase in [4Fe4S] cluster absorbance associated with oxidation (inset at right). (**b**) Y108A showed a broad, irreversible peak around -50 mV associated with $[3Fe4S]^{+}$ cluster formation; this peak underwent a proportional increase in size relative to the main peak after oxidation, and the signal decreased and fully disappeared after two hours of incubation. The UV-visible spectra of oxidized Y1078A showed evidence of aggregation (an elevated absorbance at 800 nm and a U-shaped spectrum), consistent with cluster degradation and aggregation of disassembled complexes. Electrolysis was performed with 500 nM Pol δ in storage buffer and 5.0 μM PCNA present. SQWV was performed at 15 Hz frequency and 25 mV amplitude.

Activity Assays with Electrochemically Oxidized Pol δ Mutants

To see if Y1078A and W1053A were capable of the reversible oxidative stalling seen in unmodified Pol δ DV, we carried out activity assays following electrolysis under anaerobic conditions. Anaerobic conditions were used to prevent the degradation seen in aerobically oxidized Y1078A, and all assays were run in previously degassed buffers. In contrast to aerobic oxidation experiments with Y1078A, bulk electrolysis at 0.412 mV vs NHE gives minimal yields for this mutant in an anaerobic environment (Figure 6.9). Consistent with minimal or no cluster oxidation, activity levels are indistinguishable from those of untreated anaerobic samples (Figure 6.10). Unsurprisingly, reduction of the same protein stock at -0.188 mV vs NHE had no effect, and DNA synthesis by all three samples overlay almost perfectly even across three replicates (Figure 6.10). Although the stability of this mutant is certainly lower than WT, the fact that activity levels do not change between a 20-minute oxidation and an additional 20-minute reduction indicates that complex formation was not affected under these conditions.

Unexpectedly, W1053A underwent extensive oxidation at 0.412 V vs NHE based on bulk electrolysis yields (Figure 6.9). As with unmodified Pol δ DV, oxidized W1053A shows a decrease in activity, although the difference is much greater (Figure 6.10). Notably, re-reduction does not restore activity in this mutant. Taken together, the high susceptibility to oxidation and its irreversible nature suggest complex degradation. This was somewhat unexpected under anaerobic conditions, but follows the general trend seen in aerobic electrochemistry of this mutant.

In summary, the inertness of Y1078A in the absence of oxygen is consistent with disruption of the CT pathway by this mutation. Considered alongside our aerobic electrolysis experiments, it appears that this mutant may be more sensitive to oxygen than WT Pol δ, and we

were interested in observing the response of Y1078A yeast cells to oxidative stress conditions. In contrast, all of our experiments point to CT deficiency in W0153A as being due to structural instability rather than a break in the CT pathway. Nonetheless, we were still interested in the ability of Pol δ W1053A to permit yeast survival under oxidative stress, and we thus proceeded to *in vivo* experiments with both mutants.

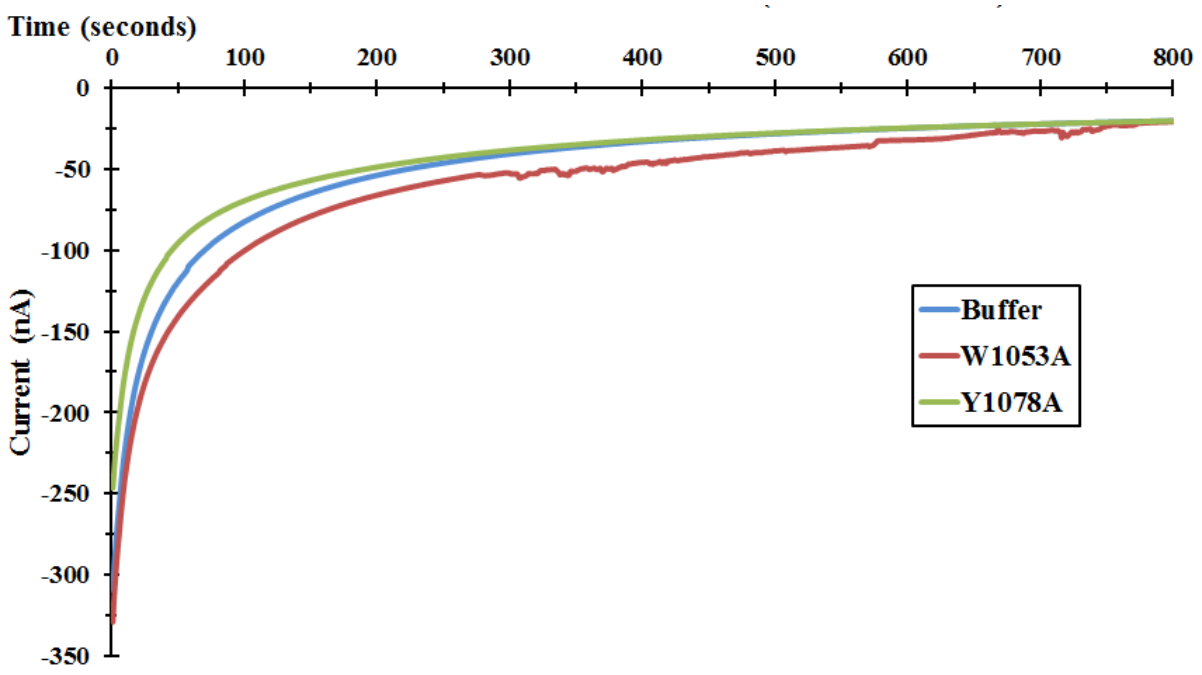

Figure 6.9 Anaerobic bulk electrolysis traces of 190 nM Pol δ DV W1053A (red) and Y1078A (green) compared to buffer trace (blue). Under anaerobic conditions, Y1078A was insensitive to oxidation, with charge yields below buffer background. W1053A unexpectedly underwent near-complete oxidation, as evidenced by the increased area under the curve relative to buffer alone. Electrolysis was carried out at 0.412 V vs NHE on a gold rod electrode, with polymerase diluted to 190 nM in degassed storage buffer (20 mM HEPES, pH 7.4, 350 mM NaAc, 1 mM DTT, 0.5 mM EDTA, 10% glycerol v/v, 0.01% decaethylene glycol monododecyl ether v/v).

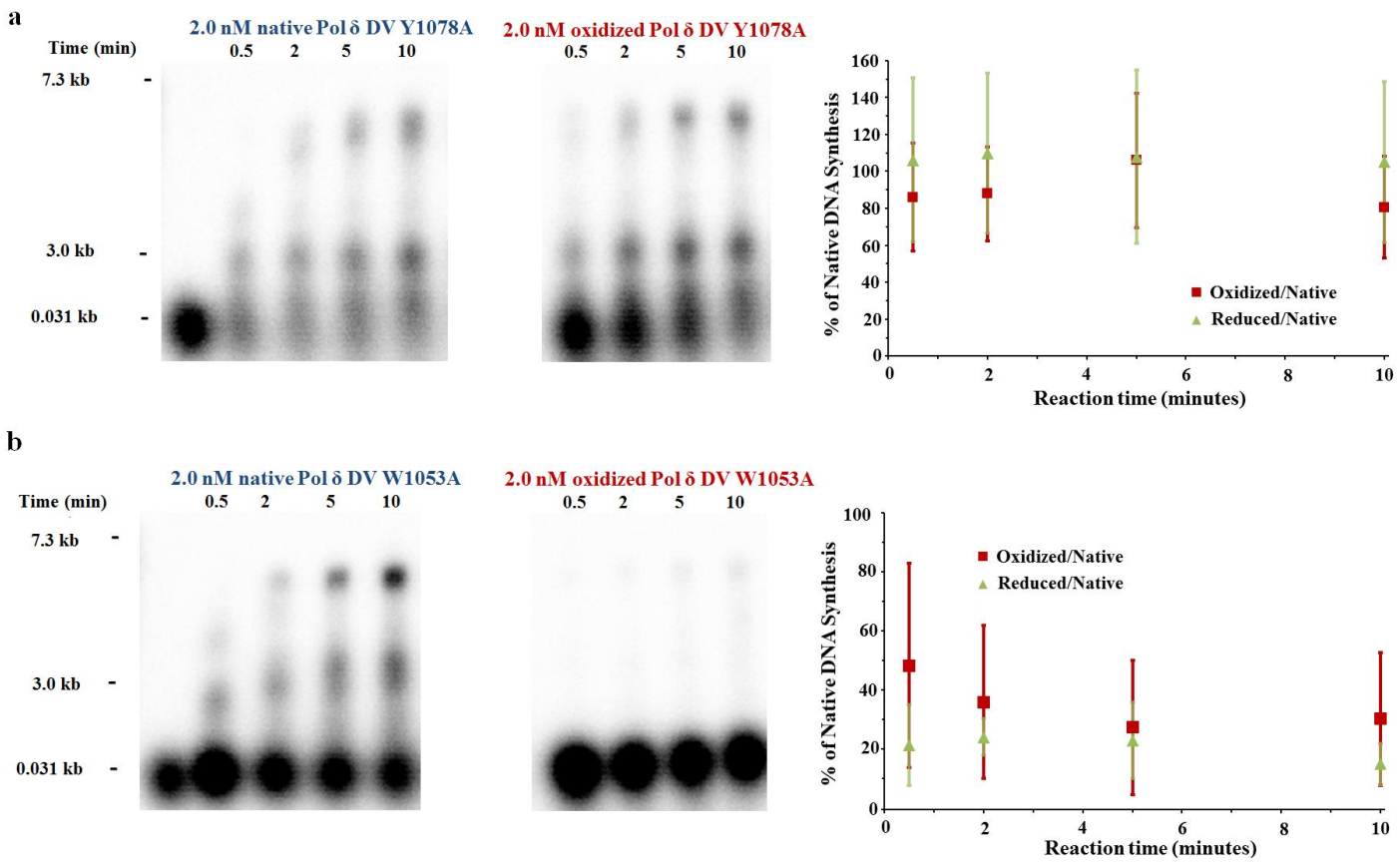

Figure 6.10 Alkaline agarose gels (left) and quantification of DNA synthesis (right) by oxidized or re-reduced Pol δ DV Y1078A (**a**) and W1053A (**b**). (**a**) Y1078A was insusceptible to oxidation (Figure 6.9), and activity of both oxidized and "re-reduced" samples were indistinguishable. (**b**) W1053A, which underwent complete oxidation (Figure 6.9), showed a pronounced loss of activity. Unlike unmodified Pol δ DV, re-reduction could not restore activity, indicating that this mutant is susceptible to cluster degradation and complex disassembly even under anaerobic conditions. Oxidation was performed by bulk electrolysis at 0.412 V vs NHE, while reduction was carried out on the same electrode at -0.188 V vs NHE. Quantification is the total DNA synthesis by oxidized or re-reduced sample divided by that of native, or untreated, sample. Error bars are the standard deviation of the mean of 3 separate experiments.

Evaluating the Sensitivity of Yeast Containing Pol δ Mutations to Oxidative Stress

In order to determine the effect of Y1078A and W1053A in cells under conditions of oxidative stress, cells were treated with exogenous H_2O_2 and spot plated. Unfortunately, no significant differences in cell survival were apparent even at low (2 mM) concentrations (data not shown), so we sought an alternative method to sensitize cells to oxidative stress. In an effort to enhance the differential in survival, the GSH2 gene was knocked out from yeast cells. GSH2 encodes glutathione synthetase; since glutathione plays a critical role in maintaining a reducing environment, this modification was expected to make cells much more susceptible to H_2O_2 treatment. Once prepared, *Δgsh* cells were treated with either 2 mM H_2O_2 or 50 mM menadione salt to induce oxidative stress (Figure 6.11). Menadione, which is a superoxide dismutase inhibitor, was included to provides an internally focused source of oxidative stress, which we thought might be more effective than H_2O_2. *Δgsh* cells proved to be very sensitive to both treatment, but cell death is so rapid in all cases that no consistent differences in survival can be observed even at H_2O_2 concentrations as low as 2 mM (Figure 6.11). In summary, these results are equivocal due to extremely rapid and non-selective cell death. Indeed, the cell-wide effects of the oxidants used is certain to enhance background effects, making the likelihood of observing differences in DNA replication responses much lower than ideal.

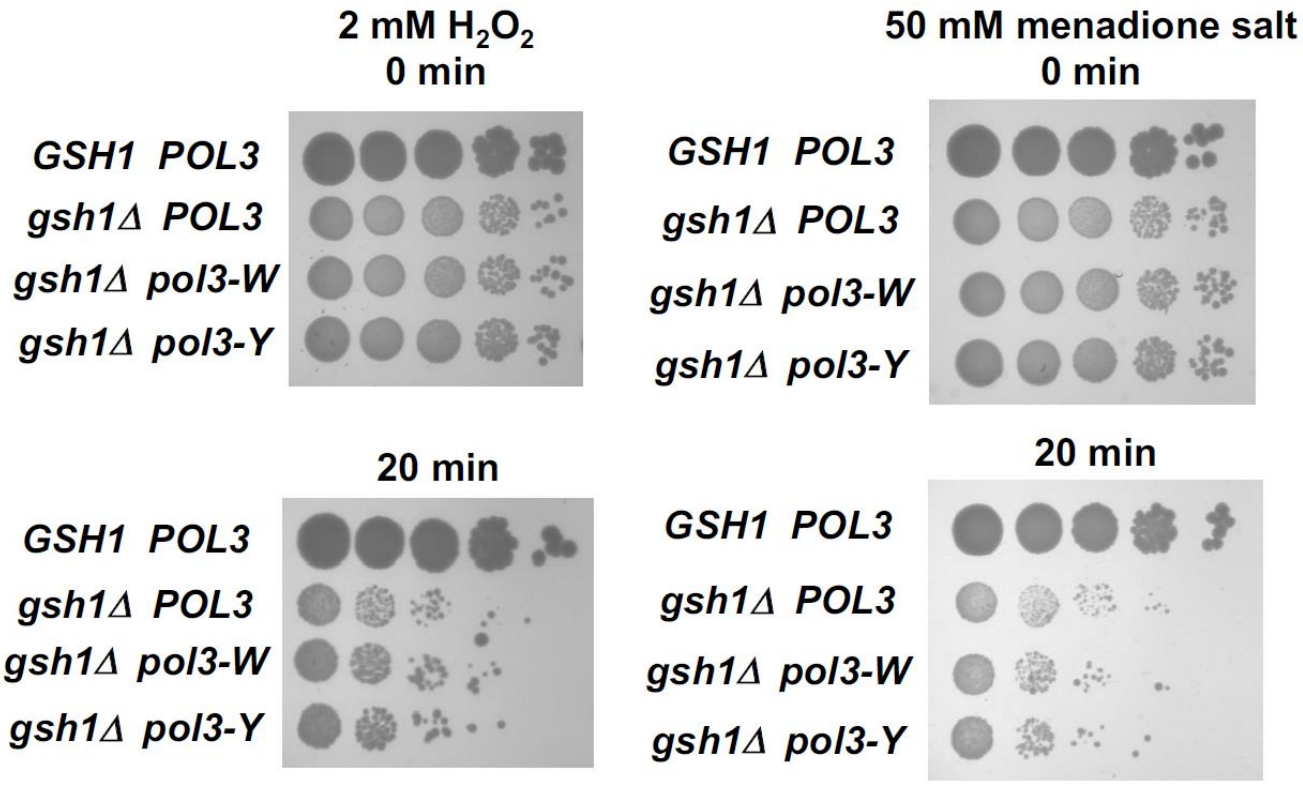

Figure 6.11 Growth of glutathione-deficient yeast strains containing WT or CT-defective Pol δ before (0 min) and after (20 min) treatment with either 2 mM H_2O_2 (left) or 50 mM menadione (right) to induce oxidative stress conditions. No consistent growth defect was observed for either Y1078A or W1053A cells, although both strains were more generally sensitive to oxidants than cells with no defects in glutathione production (top row). The lack of differences is most likely attributable to indiscriminate and delocalized cellular damage, with any actual sensitivity due to polymerase mutations masked by these non-specific effects.

Discussion

In these studies, we have attempted to identify and evaluate aromatic residues near the Pol δ [4Fe4S] cluster that might play a role in the electron transfer pathway between the cluster and DNA. From sequence alignments and comparison with a Pol α structure, we identified two residues within 15 Å of the cluster, W1053 and Y1078. The alanine mutations of both residues could be purified as intact 3-subunit complexes and retained processive activity in the presence of DNA, although multiple lines of evidence point to these mutants being less stable than WT Pol δ. Electrochemically, both were markedly CT-deficient relative to unmodified Pol δ DV, and both showed some oxygen sensitivity. Y1078A was largely redox-inert in the absence of oxygen, and showed no differences in activity after attempted anaerobic oxidation. In contrast, W1053A degraded upon bulk electrolysis even under anaerobic conditions, making the role of this residue in CT unclear. Preliminary *in vivo* studies designed to test the effect of these mutations on the oxidative stress response in yeast were similarly equivocal, with both exogenous and endogenously-induced oxidants indiscriminately killing cells too quickly for survival differences to be assessed.

Overall, these studies illustrate the challenges associated with making mutations in aromatic residues in the Pol3 C-terminal domain. While inconclusive, our work nonetheless represents a start to addressing interesting questions about Pol δ, including the role of the cluster in responding to oxidative stress and the composition of the electron transfer pathway between DNA and the cluster. It is likely that the structural instability that hindered these studies could be mitigated by using mutations to phenylalanine rather than alanine, as has been successfully done for human DNA primase (*12*). In particular, our results with Y1078A suggest that future studies would benefit from a more isomorphic mutation. With respect to the *in vivo* assays, the overall

strategy is worth pursuing with more stable mutants. However, our current results do not provide conclusive evidence for a role of the [4Fe4S] cluster in responding to oxidative stress. These failures can, however, provide a guide for more successful future experiments. The major problem with the studies as described is in the generic nature of the cellular damage. The nucleus is not a specific target for either H_2O_2 or menadione-generated superoxide, and both will indiscriminately damage biomolecules throughout the cell (*24*). One possible means of enhancing the readout of Pol δ-specific effects is S-phase synchronization and release, which would at least ensure that all affected cells were undergoing DNA replication (*25*). In addition, switching the oxidant from indiscriminate oxidizing species to photosensitizers, such as the singlet oxygen-generators Rose Bengal and methylene blue, may be of benefit in addressing the issue of the *in vivo* function of the cluster (*26*).

The importance of building on this work is emphasized by the occurrence of disease-relevant mutations in this region of Pol δ. Mutations in this critical region are rare, although the yeast Pol3-13 allele, which contains a serine in place of cysteine as one [4Fe4S] cluster ligand, is synthetic lethal with mutations in ISC machinery (*1*). Most relevant to the mutants investigated here, a case of pediatric lymphoid cancer with an R1053C mutation in Pol3 has recently been described (*27*). Arginine 1053 is two residues away from W1055, and thus has the potential to be involved in DNA binding or hydrogen bonding networks near the cluster. It will thus be of interest to repeat the experiments described herein with phenylalanine mutants, and to conduct similar experiments on Pol3-13 and R1053C.

References

1) Netz, D. J. A.; Stith, C. M.; Stümpfig, M.; Köpf, G.; Vogel, D.; Genau, H. M.; Stodola, J. L.; Lill, R.; Burgers, P. M. J.; Pierik, A. J. Eukaryotic DNA polymerases require an iron-sulfur cluster for the formation of active complexes. *Nat. Chem. Biol.* **2012**, *8*, 125 – 132.

2) Bartels, P.L.; Stodola, J.L.; Burgers, P.M.J.; Barton, J.K. A Redox Role for the [4Fe4S] Cluster of Yeast DNA Polymerase δ. *J. Am. Chem. Soc.* **2017**, *139*, 18339 – 18348.

3) Arnold, A.R.; Grodick, M.A.; Barton, J.K. DNA Charge Transport: from Chemical Principles to the Cell. *Cell Chem. Biol.* **2016**, *23*, 183 – 197.

4) Thayer, M.M.; Ahern, H.; Xing, D.; Cunningham, R.P.; Tainer, J.A. Novel DNA binding motifs in the DNA repair enzyme endonuclease III crystal structure. *The EMBO J.* **1995**, *14*, 4108 – 4120.

5) Guan, Y.; Manuel, R.C.; Arvai, A.S.; Parikh, S.S.; Mol, C.D.; Miller, J.H.; Lloyd, R.S.; Tainer, J.A. MutY catalytic core, mutant, and bound adenine structures define specificity for DNA repair enzyme superfamily. *Nat. Struct. Biol.* **1998**, *5*, 1058 – 1064.

6) Fan, L.; Fuss, J.O.; Cheng, Q.J.; Arvai, A.S.; Hammel, M.; Roberts, V.A.; Cooper, P.K.; Tainer, J.A. XPD Helicase Structure and Activities: Insights into the Cancer and Aging Phenotypes from XPD Mutations. *Cell* **2008**, *133*, 789 – 800.

7) Vaithiyalingam, S.; Warren, E.M.; Eichman, B.F.; Chazin, W.J. Insights into Eukaryotic DNA priming from the structure and functional interactions of the 4Fe-4S cluster domain of human DNA primase. *Proc. Natl. Acad. Sci. USA* **2010**, *107*, 13684 – 13689.

8) Fromme, J.C.; Verdine, G.L. Structure of a trapped endonuclease III-DNA intermediate. *The EMBO J.* **2003**, *22*, 3461 – 3471.

9) Fromme, J.C.; Bannerjee, A.; Huang, S.J.; Verdine, G.L. Structural basis for removal of adenine mispaired with 8-oxoguanine by MutY adenine DNA glycosylase. *Nature* **2004**, *427*, 652 – 656.

10) Zhou, C.; Pourmal, S.; Pavletich, N.P. Dna2 nuclease-helicase structure, mechanism, and regulation by RPA. *eLIFE* **2015**, 4:e09832.

11) Romano, C.A.; Sontz, P.A.; Barton, J.K. Mutants of the Base Excision Repair Glycosylase, Endonuclease III: DNA Charge Transport as a First Step in Lesion Detection. *Biochemistry* **2011**, *50*, 6133 – 6145.

12) O'Brien, E.; Holt, M.E.; Thompson, M.K.; Salay, L.E.; Ehlinger, A.C.; Chazin, W.J.; Barton, J.K. The [4Fe4S] cluster of human DNA primase functions as a redox switch using DNA charge transport. *Science* **2017**, *355*, 813.

13) Gray, H.B.; Winkler, J.R. Electron flow through metalloproteins. *Biochimica et Biophysica Acta* **2010**, *1797*, 1563 – 1572.

14) Dey, A.; Jenney, F.E., Jr.; Adams, M.W.W.; Babini, E.; Takahashi, Y.; Fukuyama, K.; Hodgson, K.O.; Hedman, B.; Solomon, E.I. Solvent Tuning of Electrochemical Potentials in the Active Sites of HiPIP Versus Ferredoxin. *Science* **2007**, *318*, 1464 – 1468.

15) Ha, Y.; Arnold, A.R.; Nuñez, N.N.; Bartels, P.L.; Zhou, A.; David, S.S.; Barton, J.K.; Hedman, B.; Hodgson, K.O.; Solomon, E.I. Sulfur K-Edge XAS Studies of the Effect of DNA Binding on the [Fe4S4] Site in EndoIII and MutY. *J. Am. Chem. Soc.* **2017**, *139*, 11434 – 11442.

16) Fortune, J.M.; Stith, C.M.; Kissling, G.E.; Burgers, P.M.; Kunkel, T.A. RPA and PCNA suppress formation of large deletion errors by yeast DNA polymerase δ. *Nucleic Acids Res.* **2006**, *34*, 4335 – 4341.

17) Ayyagari, R.; Impellizzeri, K.J.; Yoder, B.L.; Gary, S.L.; Burgers, P.M. A mutational analysis of the yeast proliferating cell nuclear antigen indicates distinct roles in DNA replication and repair. *Mol. Cell. Biol.* **1995**, *15*, 4420 – 4429.

18) Gomes, X.V.; Gary, S.L.; Burgers, P.M. Overproduction in *Escherichia coli* and characterization of yeast replication factor C lacking the ligase homology domain. *J. Biol. Chem.* **2000**, *275*, 14541 – 14549.

19) Henricksen, L.A.; Umbricht, C.B.; Wold, M.S. Recombinant replication protein A: expression, purification, and functional characterization. *J. Biol. Chem.* **1994**, *269*, 11121 – 11132.

20) Slinker, J.D.; Muren, N.B.; Gorodetsky, A.A.; Barton, J.K. Multiplexed DNA-Modified Electrodes. *J. Am. Chem. Soc.* **2010**, *32*, 2769 – 2774.

21) Klinge, S.; Núñez-Ramírez, R.; Llorca, O.; Pellegrini, L. 3D architecture of DNA Pol α reveals the functional core of multi-subunit replicative polymerases. *EMBO J.* **2009**, *28*, 1978 – 1987.

22) Boon, E.M.; Salas, J.E.; Barton, J.K. An Electrical Probe of Protein-DNA Interactions on DNA-Modified Surfaces. *Nat. Biotechnol.* **2002**, *20*, 282 – 286.

23) McDonnell, K.J.; Chemler, J.A.; Bartels, P.L.; O'Brien, E.; Marvin, M.L.; Ortega, J.; Stern, R.H.; Raskin, L.; Li, G.; Sherman, D.H.; Barton, J.K.; Gruber, S.B. A Human MUTYH Variant Linking Colonic Polyposis to Redox Degradation of the $[4Fe4S]^{2+}$ Cluster. **2018**, *Submitted*.

24) Imlay, J.A. Pathways of Oxidative Damage. *Annu. Rev. Microbiol.* **2003**, *57*, 395 – 418.

25) Breeden, L.L. Apha-Factor Synchronization of Budding Yeast. *Methods Enzymol.* **1997**, *283*, 332 – 341.

26) Kochevar, I.E.; Redmond, R.W. Photosensitized Production of Singlet Oxygen. *Methods Enzymol.* **2000**, *319*, 20 – 28.

27) Ma, X.; Edmonson, M.; Yergeau, D.; Muzny, D.M.; Hampton, O.A.; Rusch, M.; Song, G.; Easton, J.; Harvey, R.C.; Wheeler, D.A.; Ma, J.; Doddapaneni, H.; Vadodaria, B.; Wu, G.; Nagahawatte, P.; Carroll, W.L.; Chen, I.-M.; Gastier-Foster, J.M.; Relling, M.V.; Smith, M.A.; Devidas, M.; Guidry Auvil, J.M.; Downing, J.R.; Loh, M.L.; Willman, C.L.; Gerhard, D.S.; Mullighan, C.G.; Hunger, S.P.; Zhang, J. Rise and fall of subclones from diagnosis to relapse in pediatric B-acute lymphoblastic leukaemia. *Nat. Commun.* **2016**, *6*, 6604.